ACS APPLIED MATERIALS & INTERFACES

www.acsami.org Research Article

Unveiling the Synergistic Role of Oxygen Functional Groups in the Graphene-Mediated Oxidation of Glutathione

Yan Wang, Yasemin Basdogan, Tianyu Zhang, Ronald S. Lankone, Alexa N. Wallace, D. Howard Fairbrother, John A. Keith, and Leanne M. Gilbertson*

Cite This: https://dx.doi.org/10.1021/acsami.0c11539 Read Online

ACCESS | Metrics & More | Article Recommendations | Supporting Information

ABSTRACT: This is the first report of an atomic-scale direct oxidation mechanism of the thiol group in glutathione (GSH) by epoxides on graphene oxide (GO) at room temperature. The proposed reaction mechanism is determined using a coupled experimental and computational approach; active sites for the reaction are determined through examination of GO surface chemistry changes before and after exposure to GSH, and density functional theory (DFT) calculations determine the reaction barriers for the possible GO−GSH reaction schemes. The findings build on the previously established catalytic mechanism of GSH oxidation by graphenic nanocarbon surfaces and importantly identify the direct reaction mechanism which becomes important in low-oxygen environments. Experimental results suggest epoxides as the active sites for the reaction with GSH, which we confirm using DFT calculations of reaction barriers and further identify a synergism between the adjacent epoxide and hydroxyl groups on the GO surface. The direct oxidation mechanism at specific oxygen sites offers insight into controlling GO chemical reactivity through surface chemistry manipulations. This insight is critical for furthering our understanding of GO oxidative stress pathways in cytotoxicity as well as for providing rational material design for GO applications that can leverage this reaction.

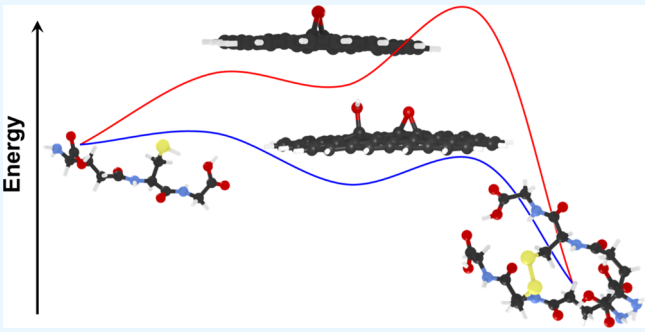

KEYWORDS: *graphene oxide, epoxide, hydroxyl, thiol, disulfide, density functional theory (DFT)*

■ INTRODUCTION

Graphene-based nanomaterials have attracted great interest in areas of drug delivery, biosensing, tissue engineering,[1−4] and more recently, to enhance agricultural crop production and to enable novel sensing capabilities to reduce stress-related loss.[5−7] Critical atomic-scale interactions between the material surface and the surrounding environment drive larger scale bio−interface interactions that enable all of these applications and potentially introduce adverse unintended consequences. Decades of research efforts have been devoted to uncovering mechanistic-level insights into cytotoxic effects[8−10] and critically to provide a rational, safe material design paradigm.[11−13] Yet, uncovering refined mechanisms for fundamental nano−bio interface interactions is fraught with challenges.

The inherent structure of graphene—composed of 2D and hexagonally arranged sp^2-bonded carbon atoms—induces attractive thermal and electrical conductivity, mechanical strength, and high surface area.[14] Graphene oxide (GO) is a graphene derivative containing various oxygen functional groups, including epoxide (C−O−C) and hydroxyl (OH) groups on the basal planes and carbonyl (C═O) and carboxylic acid (COOH) groups at the edges.[15−17] These hydrophilic oxygen groups enhance GO's aqueous phase dispersion and stability compared to hydrophobic graphene, which facilitates biophysicochemical interactions with the surrounding environment and at the nano−bio interface. The nature of these critical interactions and the resulting impact depend on the particular system of interest, which can range from whole cells[18−21] to single biomolecules.[8,22,23] Furthermore, they reveal insights that are necessary to advance promising applications that rely on these interactions as well as information about safe material design to preclude unintended consequences.[4]

Studying the impact of GO on whole cells provides information about potential adverse consequences that will result from exposure. Yet, the complexity of these systems—the organism itself and the surrounding media—makes elucidation of the mechanism challenging. Studying specific biomolecule interactions using model systems, as pursued herein, allows explicit examination of atomic-scale features and

Received: June 25, 2020
Accepted: September 17, 2020
Published: September 17, 2020

their impact on reaction mechanisms. Computational approaches, such as Kohn−Sham density functional theory (KS-DFT) or molecular dynamics (MD) simulations, can be used to provide insights into molecular interactions and validate mechanistic hypotheses.[24] Interfacial systems can be modeled as periodic systems[25] or with molecular clusters.[26] Several DFT studies have explored the importance of oxygen functional groups on the GO surface using periodic calculations. Notably, Boukhvalov *et al.* used the oxidation of benzyl alcohol to benzaldehyde as a model reaction and identified diol formation from epoxide ring opening.[27] Chen *et al.* showed that in a sodium hydroxide solution, the Na^+ cation and the water molecule assist the epoxide ring-opening reaction,[28] and Cen *et al.* studied the oxidation of SO_2 and NO by epoxide groups on GO *via* the ring-opening reaction.[25] These studies demonstrated the importance and unique reactivity of epoxide groups, particularly, to the ring opening reaction. There is also evidence that hydroxyl groups, in conjunction with epoxides, decrease the activation barriers[25,27] by creating hydrogen bonds that stabilize the transition state structures.[29] Even though GO reactions with many different chemical compounds have been studied, GO reactions with biomolecules (*i.e.*, relatively bigger molecules) have been largely unexplored.

This study tests glutathione (GSH), a thiol-rich tripeptide that is critical to the healthy function of eukaryotic and mammalian cells.[30−33] GSH serves as a predominant antioxidant enzyme to maintain the redox environment of cells and protect against the cellular oxidative stress by scavenging the free radicals that damage other important cellular components (*e.g.*, DNA, protein, and so forth).[34−37] GSH will oxidize to form glutathione disulfide (GSSG) and the balance of GSH and GSSG acts as the predictor of the cell redox state and the cell capability to defend against oxidative stress.[37,38] The measured levels of GSH have been connected with several cancers, Parkinson's disease, Alzheimer's, and HIV.[35,36] Because of the close relevance of GSH to oxidative stress, acellular GSH oxidation is commonly used to probe the level of oxidative stress imparted by graphene family nanomaterials and further to evaluate their relative adverse biological impacts.[15,34,39−43]

The mechanism(s) underlying the interaction between GO and GSH remain unresolved. Liu *et al.* proposed an O_2-mediated, two-step catalytic mechanism for GSH oxidation on graphenic nanocarbon surfaces in which (i) O_2 selectively adsorbs at carbon active sites (edge or defect sites) to form the surface oxides, followed by (ii) direct oxidation of GSH by the surface oxides or liberation of reactive oxygen species that subsequently oxidize GSH.[40] Yet, the role of surface oxygen groups already on carbon surfaces—as is the case for GO—in GSH oxidation remains unknown. Our previous research demonstrates varying oxidative potential toward GSH depending on the abundance and the specific type of oxygen groups on both carbon nanotubes[41,44] and GO.[15] GSH has been used as a "green" reducing agent to produce reduced GO or graphene, though the reduction mechanism has not been proposed.[45] The interaction between GO and GSH is known to result in the reduction of surface oxygen groups, which suggests that GO could promote GSH oxidation *via* both a (i) catalytic mechanism, whereby the carbon surface is restored after the reaction, as proposed by Liu, *et al.*[40] and (ii) direct oxidation in which GO oxidizes GSH resulting in a change in the surface chemistry.

We now interrogate these mechanisms with experiment and computational theory to resolve the influence of highly reactive and abundant epoxide groups on GSH oxidation. Specifically, we uncover the relative energetics of elementary reactions involving the different oxygen surface groups (*i.e.*, C−O−C, C−OH, C═O, and COOH). As the amount and type of surface oxygen groups can be manipulated in a semicontrolled manner, knowing the role of each functional group in this mechanism provides a rational design paradigm. The active oxygen groups involved in the direct oxidation of GSH were determined by examining the GO surface chemistry before and after the reaction with GSH using X-ray photoelectron spectroscopy (XPS). GO samples with different atomic percent oxygen and oxygen compositions (*i.e.*, relative abundance of different surface groups and the presence and absence of epoxide groups, specifically) were reacted with GSH. These empirical results were combined with DFT calculations to propose the mechanism of interaction. Refined modeling of chemical reactions requires full exploration of accessible regions of phase space using MD simulations,[46] but these can be prohibitively costly to run, especially when used for investigating larger scale systems such as GSH oxidation. As a first step toward identifying essential elementary mechanisms, we used a static DFT calculation scheme with explicit solvent molecules to quantify reaction barriers for different possible GO−GSH reaction schemes in order to identify the preferred reactions between specific oxygen groups and GSH. To our knowledge, this is the first molecular-scale study of GO−GSH reaction mechanisms. This work also opens the door for other detailed mechanism analyses of a plethora of other biologically important thiol-containing biomolecules (*e.g.*, cysteine) and drugs (*e.g.*, captopril), as well as other important nano−bio interface mechanisms (*e.g.*, membrane lipid peroxidation, the initial point of nanomaterial−cell contact).

RESULTS AND DISCUSSION

GSH Oxidation Mediated by GO Proceeds *via* Parallel Catalytic and Direct Oxidation Routes. GSH oxidation to GSSG (Figure S1) is a critical intracellular biochemical reaction that proceeds to reduce oxidative species that would otherwise induce cellular oxidative stress.[37] This reaction was previously proposed to occur *via* a catalytic mechanism involving dissolved oxygen (DO),[40] which we confirm (Figure 1) for our system (as-received GO (ARGO), synthesized by modified Hummer's method) under ambient DO conditions (~0.26 mM). The oxidative potential of ARGO toward GSH after five successive cycles is repeatable, exhibiting a typical catalytic behavior. These experiments also identified near complete GSH removal at an incubation time of 12 h under ambient DO conditions for $[GSH]_0$ = 0.33 mM.

To investigate the potential direct reaction between GSH and surface oxygen groups of GO, a low DO condition (~0.008 mM) was used (see details in the Materials and Methods section). GSH (0.33 mM) exposed to 0.05 mg mL^{-1} of ARGO under ambient DO conditions for 6 h produced 0.09 mM of GSSG (Figure 2a) corresponding to a 54% loss of GSH (Figure 2b), consistent with our findings presented in Figure 1. When this experiment was repeated under low DO conditions, the percent loss of GSH decreased to 20% (Figure 2b), which suggests that the oxidation of GSH by GO is predominantly driven by the DO-mediated catalytic mechanism. We anticipate that the catalytic mechanism likely persists under low DO conditions, though to a significantly reduced degree.

https://dx.doi.org/10.1021/acsami.0c11539
ACS Appl. Mater. Interfaces XXXX, XXX, XXX−XXX

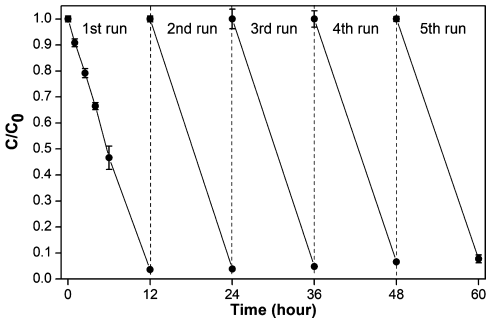

Figure 1. GSH oxidation repeated for five cycles under ambient DO conditions. Fresh GSH stock was added to the same reaction vial after each 12 h cycle. C_0 is the initial concentration of GSH and C is the concentration after "t" h of incubation. The depletion of GSH was measured using Ellman's assay. The concentration of ARGO was 0.05 mg mL^{-1} and the initial GSH concentration for each cycle was 0.33 mM. Sampling was conducted at multiple time points (0, 0.5, 1, 2.5, 4, 6, and 12 h) for the first cycle while only at the beginning and end of subsequent cycles. Samples were run in triplicate (n = 3) and the error bars represent the standard deviation of measurements.

Still, the 20% loss of GSH under low DO conditions suggests that a second, direct oxidation mechanism may be at play.

The lack of significant difference (two-sample t-test, p > 0.05) in total glutathione (GSH + GSSG) between the ARGO and control (no ARGO added) samples indicates that GSSG is the dominant oxidation product (Figure 2a). GSH can be oxidized to minor higher oxidation byproducts, such as sulfinic (R−SO(OH)) and sulfonic (R−S(=O)$_2$−OH) acids.[40,47] However, unlike GSSG, these higher oxidation byproducts cannot be reduced to GSH through the addition of glutathione reductase.[48,49] If these higher oxidation byproducts are formed, the amount of total glutathione (GSH + GSSG) in the reaction mediated by ARGO would be lower than that of the control, which we do not observe in our data (Figure 2a).

Quantifying Changes in GO Surface Chemistry before and after Exposure to GSH Indicates a Possible Direct Reaction with Epoxide Groups. The potential for a direct reaction (noncatalytic) between GSH and oxygen functional groups on the surface of GO was pursued by quantifying changes in the GO surface chemistry before and after exposure under low DO conditions. A range of GSH concentrations (3.3−33.3 mM) and incubation times (0−36 h) were investigated to account for potential concentration and time influence on the direct interaction between oxygen groups on the GO surface and GSH. The higher concentrations and longer exposure times ensured measurable changes of GO surface chemistry.

As expected, increased GSH concentrations and exposure times both result in higher absolute loss of GSH *via* ARGO-mediated oxidation (Figure 3, circles). At the end of each experiment, samples were isolated, extensively washed (referred to as post-ARGO or P-ARGO), and characterized by XPS (results summarized in Figure 4). The XPS data of the

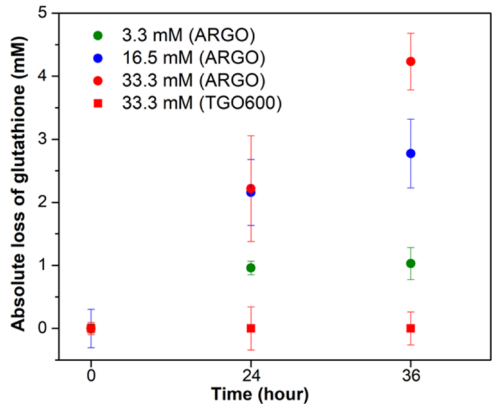

Figure 3. Absolute loss of GSH with different initial concentrations of GSH (3.3, 16.5, and 33.3 mM) by ARGO (green, blue, and red circles, respectively) and TGO600 (red squares) under low DO conditions for a total incubation time of 36 h. The loss of GSH was measured using Ellman's assay, and the concentration of GO was 0.05 mg mL^{-1}. Samples were run in triplicate (n = 3) and the error bars denote the standard deviation of measurements.

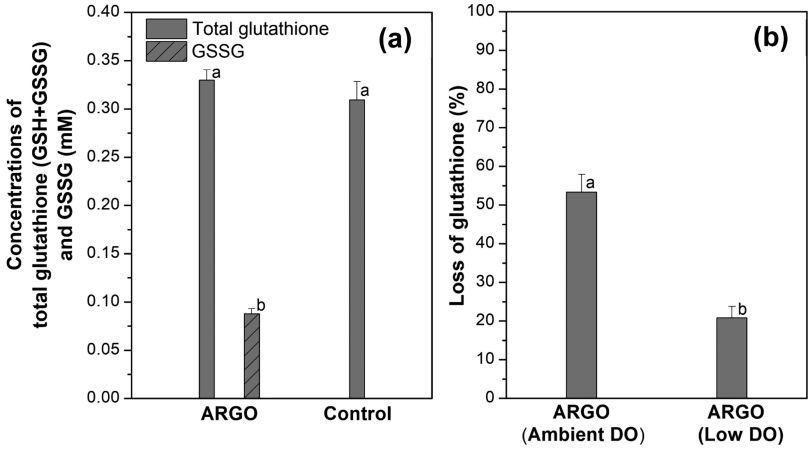

Figure 2. (a) Total glutathione (GSH + GSSG) and GSSG measurements using the GSSG/GSH quantification kit assay after incubation with ARGO for 6 h under ambient DO conditions (~0.26 mM). The amount of GSSG was quantified by adding glutathione reductase to the experimental system at 6 h to reduce GSSG to GSH (unreacted, free GSH was protected prior to the addition of glutathione reductase). (b) Percent loss of GSH under ambient and low DO conditions (~0.008 mM) for a 6 h incubation with ARGO measured using Ellman's assay. The concentrations of ARGO and initial GSH for (a) and (b) were 0.05 mg mL^{-1} and 0.33 mM, respectively. Samples were run in triplicate (n = 3) and the error bars represent the standard deviation of measurements. Means suffixed with different letters (a, b) are significantly different from each other by the two-sample t-test (95% CI, p < 0.05).

https://dx.doi.org/10.1021/acsami.0c11539
ACS Appl. Mater. Interfaces XXXX, XXX, XXX−XXX

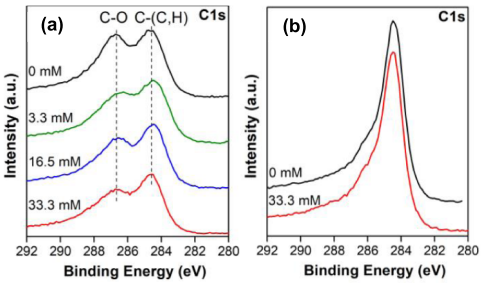

[GSH], mM	C	O	N	S	Na	O: C
P-ARGO						
0	65.6	32	0.3	0	2.1	0.488
3.3	66.5	30.5	1	0.2	1.7	0.459
16.5	66.9	30.2	0.8	0	2.1	0.451
33.3	67.7	28.7	1.3	0.2	2.1	0.424
P-TGO600						
0	85.2	14.1	0	0.1	0.6	0.165
33.3	84.9	13.9	0.6	0.4	0.2	0.164

Figure 4. XPS C 1s spectra of (a) P-ARGO and (b) P-TGO600 samples exposed to different initial concentrations of GSH (3.3, 16.5, and 33.3 mM) under low DO conditions for a total incubation time of 36 h. The sample exposed to 0 mM GSH serves as the control. The table shows changes in the atomic percent of the elemental composition and the oxygen-to-carbon atom ratio (O:C) on GO samples determined from the XPS data of samples postexposure.

C 1s region indicate that exposure to GSH results in a change in the C 1s spectral profile that is consistent with the decrease in the oxygen content of P-ARGO. In addition, the oxygen-to-carbon (O:C) ratio before and after exposure is in agreement with the change of the spectral profile (*i.e.*, loss of oxygen) as the O:C ratio decreases from 0.488 for the control P-ARGO sample (no GSH added) to 0.424 for the P-ARGO sample with a 33.3 mM initial concentration of GSH. Given the reactive nature of epoxides, the diminishment of the C−O component at ∼287 eV could indicate an epoxide ring opening leading to elimination of the epoxide group.[50] Importantly, there is no significant increase of N and S observed in the P-ARGO sample, confirming that no GSH is adsorbed to the surface and that GO−GSH conjugates (*i.e.*, other non-GSSG intermediate products, see above) are not appreciably formed in the direct reaction mechanism.

To investigate the potential of epoxide groups to play a role in the oxidation of GSH under low DO conditions, we prepared a reduced GO sample by thermally annealing ARGO up to 600 °C (TGO600). Annealing exploits the thermal stabilities of oxygen groups and was used to selectively reduce surface oxygens. Epoxides are the least thermally stable[51] and are expected to be fully reduced at 600 °C; carboxylic acid groups will also be removed due to thermal decarboxylation at this temperature.[51−53] XPS data of TGO600 indicate that thermal annealing led to extensive depletion of C−O-bound oxygen in the sample, as observed in both the decrease in the atomic concentration of oxygen (32% oxygen to 14.1% oxygen) and the corresponding loss of the C−O feature at ∼287 eV in the C 1s region (Figure 4b). The loss of oxygen and diminishment of C−O character in the C 1s region after thermal annealing at elevated temperatures are consistent with previous observations of GO transformations after thermal annealing and has been previously attributed to the loss of epoxide groups.[15,54] Furthermore, the slight shoulder persisting at ∼287 eV for TGO600 is expected, as it suggests the existence of trace residual oxygen-containing groups attributed to hydroxyl and carbonyl groups, which have higher thermal stability.[51−53] Attenuated total reflectance-Fourier transform infrared spectroscopy (ATR-FTIR) was performed to obtain further insights regarding the transformation of GO and confirms that after annealing at 600 °C, epoxide groups were absent on the GO surface. This is indicated by the absence of the peak at ∼1000 cm^{-1} in the TGO600 sample, which represents epoxide groups (C−O−C) (Figure S2).[15,50,55]

The GSH oxidation assay was repeated under low DO conditions at the highest initial GSH concentration (33.3 mM) with TGO600, and no significant loss of GSH is observed with increasing exposure time (Figure 3, squares). Furthermore, there are no significant changes in the surface chemistry (*i.e.*, the C 1s spectrum) for the postreaction TGO600 sample (P-TGO600) (Figures 4 and S2). Thus, we propose that the removal of reactive epoxide groups on the GO surface limits the direct oxidation reaction with GSH and suggest that the contribution of residual oxygen-containing groups on TGO600 (*e.g.*, C═O) to this reaction is insignificant.

The loss of oxygen on the surface of ARGO, as determined by XPS (Figure 4), can be used to estimate the contribution of the direct reaction mechanism to the loss of GSH under low DO conditions. For the 3.3 mM GSH concentration condition (Figure 3), the percent contribution of the catalytic mechanism is approximately 10 times that of the direct mechanism. While our system is not ideal (*i.e.*, some DO remains) and the relative contribution of the direct mechanism will depend on the system conditions (*e.g.*, initial GSH concentration), this estimate provides a rough baseline comparison.

The combined results corroborate our previous findings[15] that surface oxygen influences the propensity for GO to oxidize GSH under ambient DO conditions (combined catalytic and direct oxidation mechanisms). In the ambient DO system with 0.33 mM GSH, 53 and 20% loss of GSH are observed after 6 h of exposure for ARGO (Figure 2b) and TGO600 (Figure S3), respectively. The primary differences between ARGO and TGO600 include the amount of surface oxygen, exclusion of surface epoxide groups, and the changes in consequential physiochemical properties (*e.g.*, aggregation, electrical conductivity, and so forth) resulting from thermal reduction of oxygen groups, which are known to drive the catalytic mechanism.[15,40]

Determining Elementary Reaction Steps of the GO-GSH Reaction Using DFT Calculations. There are three primary components to the model evaluated in this work: graphene, surface oxygen groups, and GSH. A graphene nanoflake model was used consisting of 52 carbon atoms (forming 18 aromatic rings) with 18 capping hydrogen atoms to ensure that the model had a physically relevant spin state of S = 0. Preliminary calculations using a 31-carbon atom cluster forming 10 aromatic rings were found to be unstable due to inadequate stabilization provided by the smaller cluster. Given the reasonable structure of the moderate-sized cluster model with adsorbates relative to the smaller cluster model, we expected that an even larger cluster model would not significantly impact the calculation results. Nevertheless, we tested the viability of a larger graphene nanoflake model. Unfortunately, electronic energy optimizations for these cases

https://dx.doi.org/10.1021/acsami.0c11539
ACS Appl. Mater. Interfaces XXXX, XXX, XXX−XXX

were slow and could not be converged in a timely manner, so for practical reasons we did not do further tests on the large cluster models. Four primary oxygen groups were considered: epoxide (C−O−C) and hydroxyl (OH) groups on the basal plane, and carbonyl (C═O) and carboxylic acid (COOH) edge groups.[15−17] The GSH molecule ($C_{10}H_{17}N_3O_6S$) is a carbon chain decorated with two carbonyl, one thiol group (−SH), one amino group ($-NH_2$), and two carboxylic acid groups at either end. Molecular GSH is more stable in solution as a zwitterion (by 6.7 kcal/mol), but the zwitterion state is higher in energy in the gas phase (by 7.6 kcal/mol). Thus, solvation clearly plays an important role in stabilizing the zwitterion form of the GSH molecule. However, as solvation energies are physically expected to be less on a surface (due to the decrease in the solvent-accessible surface area upon adsorption), and because we doubt the physical validity of using a continuum solvation model with this carbon nanoflake cluster model (*vide infra*), we modeled all species as a molecular cluster using GSH based on a non-zwitterion form. All calculations were performed by modeling each reactant and product as a single cluster to maximize error cancellation. Figure 5 shows representative cluster models used in this work.

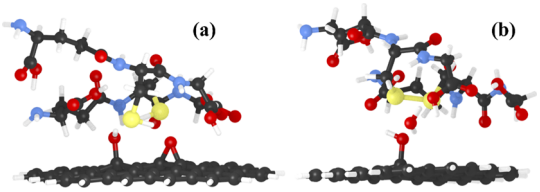

Figure 5. Representative molecular cluster models used in computational studies. (a) Reactant state with two oxygen functional groups (C−O−C and C−OH) and two GSH molecules hydrogen-bonded to the surface oxygen groups. (b) Product state with one oxygen functional group (C−OH) as well as oxidation products: water and GSSG. Atom coloring: black = carbon; white = hydrogen; red = oxygen; blue = nitrogen; and yellow = sulfur.

DFT calculations were used to assess the reaction energetics for possible reactions between different GO oxygen groups and the thiol and amino groups of GSH (Table S1). The thiol and amino groups were identified to be the most likely reaction sites (as compared to the C═O groups and C−OH in the GSH chain or COOH terminal groups) as their bonds to the carbon chain are weaker and thus more reactive.[56,57] Subsequently, the thiol group was identified as the preferred site to react with the GO surface as it has a lower S−H bond strength (~86.8 kcal/mol) compared to the N−H bond (~92.3 kcal/mol).[56,57] The relative difference in bond strengths correlates with the calculated reaction barriers (Table S1).

As a first step toward determining the reaction mechanism, reactions of GSH with the GO surface containing one epoxide, one hydroxyl, one carbonyl, or one carboxylic acid group were modeled. Calculations for reactions involving hydroxyl, carbonyl, and carboxylic groups resulted in very high barriers (greater than 50 kcal/mol) and thus were considered unfeasible. GSH deprotonation on a clean graphene surface was also considered; however, this reaction also resulted in very high barriers. Barriers involving a single epoxide group were found to be substantially lower, but the calculated reaction energies (Figure 6, reaction 1) were not consistent with experimental data that suggested GSH oxidation to be a

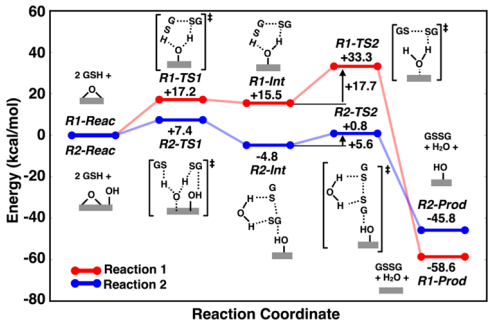

Figure 6. Calculated reaction-free energies for two different GSH oxidation reaction mechanisms identified in this work. Gas-phase reaction-free energies are reported at the ωB97x-D3/def2-TZVP//BP86-D3BJ/def2-SVP level of theory. Details of atomic-scale structures are shown in Figure 7, and *XYZ* coordinates are provided in the Supporting Information. (Reac = reactants for the reaction, TS1 and TS2 = first and second transition-state structures, and Prod = products at the end of the reaction).

facile process. The first step in reaction 1 involves the epoxide ring opening concomitant with the proton transfer from one GSH molecule, and the formation of a surface hydroxyl group is energetically uphill by 15.5 kcal/mol (R1-TS1, barrier = 17.2 kcal/mol). The subsequent proton transfer from the second GSH molecule forms a water molecule with a reaction energy of −74.1 kcal/mol (R1-TS2, barrier = 17.7 kcal/mol). Even though the overall reaction energy is calculated to be highly exothermic (−58.6 kcal/mol), the calculated barriers are too high for a reaction that is observed to occur at room temperature. The high barriers in reaction 1 result from water formation and the loss of intermolecular interactions between the surface oxygen species and the GSH molecules relative to the reactant structure (see Figure 7 and *XYZ* coordinates in the Supporting Information).

The energetics for reaction 1 seemed unlikely to reflect the actual process, so an alternative configuration of oxygen species was considered in which an epoxide was adjacent to a hydroxyl group.[25,27] Three different sites are considered when placing the hydroxyl group on the surface: one, two, and three carbon atoms away from the epoxide group. The most stable configuration was achieved when the hydroxyl group was two carbon atoms away from the epoxide (*i.e.*, 3.40 Å, see Figure 5a). In this scenario, the first step of reaction 2 is the epoxide ring-opening reaction with the proton transfer of a GSH molecule to form a diol group on the surface, but the diol group then immediately reacts with the second GSH molecule to form a metastable complex of deprotonated GSH molecules and water, which interact with the adjacent hydroxyl group. This overall process is downhill, −4.8 kcal/mol (R2-TS1, barrier height = 7.4 kcal/mol). The interatomic distance between the two sulfur atoms in the reactant state is 4.6 Å, and this increases to 5.3 Å in the intermediate state due to the formation of a stable hydrogen bond between the two sulfur atoms in the deprotonated GSH molecules and the now-formed water molecule. The second step of reaction 2, the formation of the S−S bond between the deprotonated GSH molecules, is energetically downhill, −41.0 kcal/mol (R2-TS2, barrier height = 5.6 kcal/mol). In this step, the interatomic distance between the sulfurs decreases from 5.3 to 2.1 Å, thus reflecting a GSSG molecule.

These calculation results suggest that the only energetically feasible GSH oxidation pathway does not involve a single

https://dx.doi.org/10.1021/acsami.0c11539
ACS Appl. Mater. Interfaces XXXX, XXX, XXX−XXX

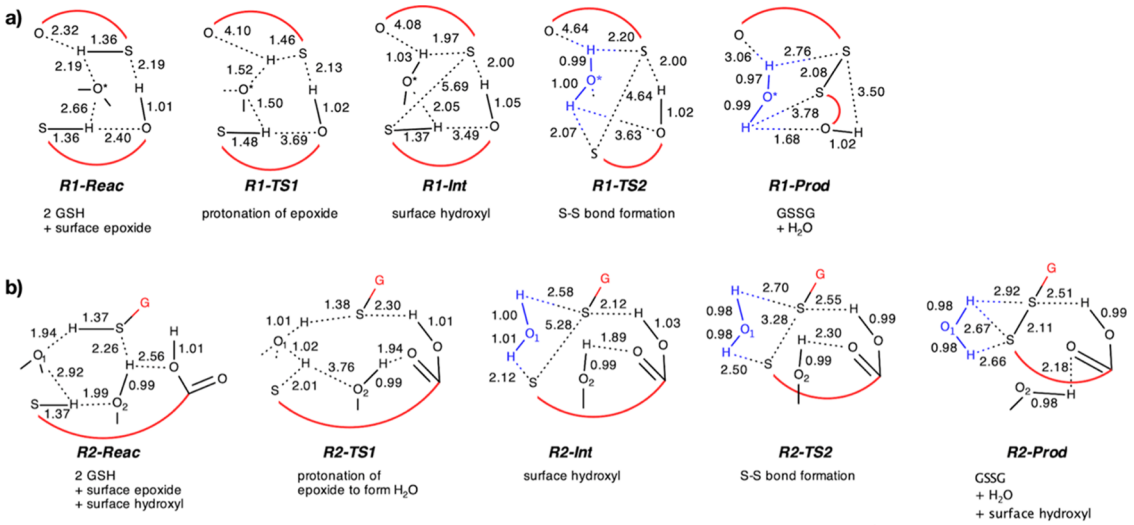

Figure 7. Selected interatomic distances (numerical values reported in Å) for GSH oxidation mechanisms shown in Figure 6. Note that atomic-scale structures are complex and interatomic distances are not drawn to scale, and *XYZ* coordinates are provided in the Supporting Information. (a) Reaction 1 species. Red curve lines are surrogates for GSH backbone structures. O* refers to a surface-bound O atom, which initially is a surface bound epoxide, then a surface-bound hydroxyl, and then a dissociated water molecule (drawn in blue). (b) Reaction 2 species. The red curved line is a surrogate for one of the GSH backbone structures and the G-group represents the remainder of another complete GSH molecule. "O_1" refers to a surface-bound O atom, which initially is a surface-bound epoxide, and then a dissociated water molecule (drawn in blue). "O_2" refers to a surface-bound OH group that remains intact throughout the reaction but participates in hydrogen bonding to facilitate the GSH oxidation steps. (Reac = reactants for the reaction, TS1 and TS2 = first and second transition-state structures, and Prod = products at the end of the reaction).

surface oxide group, in this case, the epoxide species. Instead, GSH oxidation likely occurs at a surface site that involves both a surface-bound epoxide (that eventually becomes H_2O) as well as a nearby C−OH group that forms a stabilizing interaction with a GSH molecule, allowing for a lower energy pathway for S−S bond formation. As epoxide and hydroxyl groups are present on the basal plane of GO, these two groups together play a synergistic role. The observation from our work showing that hydroxyl groups can form hydrogen bonding networks has also been observed in previous computational studies of GO.[25,27]

As this reaction is run in an aqueous solution, the impact of using continuum treatment for solvation (Figure S4) was also considered. No qualitative differences were found when a continuum solvation model was used, but there were quantitative changes to generally make intermediate energies lower and barrier heights higher. We suspect this to be an unphysical result because of the nanoflake cluster model that uses a finite graphene system with capping hydrogen atoms rather than a more physical (and more computationally costly) periodic system with an extended GO surface. While solvation energy contributions are normally assumed to be very important in homogeneous catalysis,[58,59] it usually plays a less significant role in heterogeneous catalysis studies[60] as the latter systems have much less solvent-accessible regions by virtue of being at a solid/liquid interface. Here, the role of solvent likely plays even less of a role given the relatively bulky nature of GSH molecules that would further limit the accessibility of solvent molecules beyond what the surface alone would. For this reason, in this particular case, gas-phase calculations bring more error cancellation and thus better resemble results obtained from experimental work. To make a more informative and precise conclusion on the role of solvation in GSH oxidation, explicit solvation modeling should be carried out, likely using computationally costly QM/MM MD simulations within a periodic model for the GO surface. However, avoiding this computational cost was the motivation for using this cluster model in the first place. As stated earlier, the intent for the computational work was to provide insights into the reaction process that is experimentally known to occur and, at present, the gas-phase energetics determined herein appear to be the most representative of our experimental findings.

Others have identified that sulfenic acid (G-SOH) is a key transient intermediate in the oxidation reactions of thiols and is rapidly consumed to form disulfides in the presence of thiols,[61−64] but whether it is an intermediate on GO is unknown. Computational models are used to study a single GSH molecule reacting with an epoxide group to form G-SOH, and this resulted in a moderate barrier (15.3 kcal/mol) similar to barriers found in reaction 1, but subsequent pathways were found to be highly unfavorable and greater than (50 kcal/mol). The *XYZ* coordinates of the structures used to calculate 15.3 kcal/mol barrier (reactants, transition state, and products) are given in the Supporting Information. As an analogue to reaction 2, G-SOH formation in the presence of both an epoxide and a hydroxyl group is also modeled. As seen with reaction 2, the calculated barrier became even more reasonable (8.2 kcal/mol), but after multiple attempts we could not find a reasonably low barrier for a subsequent step (all calculated barriers were found to be more than 50 kcal/mol). The GSH molecule reacting *via* the nitrogen site and forming a G-NOH_2 molecule was also considered, but the barrier calculated for this reaction (21.5 kcal/mol) was higher compared to that for G-SOH formation (15.3 kcal/mol). This is not surprising as S−H bonds are substantially weaker than N−H bonds (*vide supra*), and so it is easier for oxygen to get inserted between an S−H bond rather than an N−H bond. The list of all the studied reactions is provided in Table S1. To summarize these results, there is computational evidence that GSH oxidation to GSSG on GO may involve the formation of G-SOH, but we found no

https://dx.doi.org/10.1021/acsami.0c11539
ACS Appl. Mater. Interfaces XXXX, XXX, XXX−XXX

energetically reasonable pathways to show it as an intermediate en route to GSSG rather than a side product.

■ CONCLUSIONS

The integration of experimental and computational approaches enables obtaining new knowledge and insights into the interactions of GO and the important cellular antioxidant, GSH. The results from both approaches reveal a direct oxidation mechanism of GSH by a GO surface, which build on the previously reported catalytic oxidation mechanism. Examination of changes in the GO surface chemistry before and after exposure to GSH shows a decrease in the C−O content for a GO sample with epoxide groups (ARGO) and no notable change in the GO surface for a reduced GO sample without epoxide groups (TGO600). These experimental data suggest the important role of epoxide groups in the direct oxidation of GSH, which are further supported using computational quantum chemistry modeling. DFT calculations of possible reaction schemes between GSH and oxygen groups on GO demonstrate that epoxide groups are the preferred active sites for GSH oxidation. Furthermore, proximal hydroxyl groups play an important role in facilitating GSH oxidation by stabilizing the transition state through intermolecular hydrogen bonding interactions between the hydroxyl groups on the GO and the reacting GSH species.

The combined experimental−computational methodology enables interrogation of the direct mechanism, and the approach is transferrable to the study of surface reaction mechanisms beyond GSH. The results reveal general interaction mechanisms between oxygen-functionalized carbon nanomaterials (CNMs) and other thiol-containing molecules. Furthermore, this work provides insights into manipulating surface oxygen groups to rationally design CNMs to meet intended performance needs in an application that may or may not necessitate bioactivity. For example, the reactive sites on CNMs (*e.g.*, epoxides on GO) can be tailored to minimize their toxicity. On the other hand, the surface chemistry can be manipulated to CNM surface reactions that are important for monitoring thiol-related biological processes (*e.g.*, sensitive probes, biosensors, and so forth). While a low DO environment has allowed us to identify the direct interaction mechanisms between GSH and the GO surface, these conditions are also relevant to anoxic natural and engineered systems. For example, anoxic conditions occur in natural, subsurface water, and soil systems; our research findings not only illuminate the potential adverse impacts of unintended release of CNMs to the ecosystem but can also be used to advance the identification of thiol compounds in such environmental samples using CNM-based sensing platforms. In engineered systems (*e.g.*, microbial fuel cells, sensors, and so forth), there are opportunities to leverage nano−bio interactions to enhance the performance (*e.g.*, electron transfer, selectivity, and sensitivity of detection events). For example, in microbial fuel cells, CNM-based anode electrodes can be manipulated by changing surface chemistry to ensure biocompatibility with anaerobic microbes while still facilitating the desired extracellular electron transfer.

■ MATERIALS AND METHODS

Material Preparation. Single-layered GO, synthesized by modified Hummer's method, was purchased from ACS Materials LLC (Medford, MA, USA) and used as-received (labeled ARGO). One thermally annealed sample was prepared by heating ARGO under helium gas flow at 600 °C for 30 min and referred to as TGO600. Centrifugation was adopted to isolate and collect ARGO after exposure to GSH, while filtration was used for TGO600. These postreaction samples were cleaned with sufficient rinsing with deionized water and dried in a vacuum desiccator and labeled P-ARGO and P-TGO600, respectively. The postreaction sample without GSH exposure was used as the control.

Measurement of GSH and Its Oxidation Product GSSG. *Measurement of GSH by Ellman's Assay.* The depletion of GSH after exposure to GSH was measured under acellular conditions using Ellman's assay (DTNB, 5,5′-dithiobis (2-nitrobenzoic acid)), as described in our previous studies.[15,41,44,65] The GO suspension was prepared by 1 h bath sonication (VWR Aquasonic 150T) and added to the GSH solution in a 33 mM bicarbonate buffer (pH = 8.6) to initiate the reaction, during which the sample vials were covered with an aluminum foil to avoid potential photoinduced oxidation and rotated continuously during the experiment at room temperature. The final concentration of GO was 0.05 mg mL^{-1} and different initial concentrations of GSH (0.33, 3.3, 16.5, and 33.3 mM) were applied. GO was filtered out of the solution using a 0.22 μm syringe filter before the measurement. The concentration of free GSH in the filtered sample solution was quantified using Ellman's reagent that reacts with the thiol group of GSH to produce a yellow product 3-thio-6-nitrobenzoate, which can be detected by UV−vis spectroscopy at 412 nm.

Measurement of GSSG by the GSSG/GSH Quantification Kit Assay. The GSSG/GSH quantification kit assay (Dojindo Molecular Technologies, Inc.) was used to determine the amount of formed GSSG, while the total glutathione (GSH + GSSG) and free GSH were measured at the same time. Specifically, the filtered sample solution was incubated with DTNB and glutathione reductase for 10 min at 37 °C, whereas GSSG was converted back to GSH by glutathione reductase. Total glutathione concentration was determined by measuring the absorption at 412 nm using a 96-well microplate reader. GSSG was quantified by masking the GSH thiols with the Dojindo masking reagent that does not cause interference for the reaction of GSSG measurement according to the manufacturer's protocol. Free GSH was then calculated by subtracting GSSG from the total glutathione.

The loss of GSH and the production of GSSG were calculated with reference to the control (no GO added). As the GSH air oxidation occurs in the control leading to a small amount of GSH loss and GSSG production, all the GSH and GSSG data for the samples and the control were calibrated by subtracting the contribution of GSH air oxidation.

The GSH oxidation was conducted under ambient and low DO conditions, respectively. The ambient O_2 condition refers to the situation that DO is at a normal level (*i.e.*, 0.26 mM), while the low O_2 condition was achieved by purging the solution with nitrogen gas for 20 min before initiating the reaction, resulting in a DO level of 0.008 mM. All the experiments were performed in triplicate.

For the five-cycle experiment under ambient DO conditions (Figure 1), sampling was conducted at multiple time points (*i.e.*, 0, 1, 2.5, 4, 6, and 12 h) for the first cycle, and for the subsequent cycles, sampling was only conducted at the beginning and end of each cycle to maximize the ARGO remaining in the reaction vessels.

Characterization of Materials before and after Reaction with GSH. XPS was used to determine the elemental composition of samples and evaluate the changes in the surface oxygen groups. The spectra were collected using a PHI 5600 instrument with a Mg Kα (1253.6 eV) flood source. Powdered samples were dried in a desiccator prior to analysis and then secured with a double-sided copper adhesive tape on an XPS sample stub. After preparation, samples were introduced into an ultrahigh vacuum environment. Surveys were collected to identify the elements and ensure that there were no impurities in the samples. Quantitative analysis was performed on high-resolution multiplex spectra for the existing elements including carbon (C 1s), nitrogen (N 1s), sodium (Na 1s), oxygen (O 1s), and sulfur (S 2p) regions at a pass energy of 29.35 eV

https://dx.doi.org/10.1021/acsami.0c11539
ACS Appl. Mater. Interfaces XXXX, XXX, XXX−XXX

and a step size of 0.125 eV, with 20 sweeps per region. XPS spectra were quantitatively analyzed using CasaXPS.

ATR-FTIR spectroscopy was employed as a complementary technique to XPS to confirm the changes in the surface oxygen groups. The data were collected using a Nicolet iS5 with a diamond window. Prior to analysis, samples were dried in a desiccator for at least 24 h. Samples were analyzed from 4000 to 400 cm^{-1} at a resolution of 0.482 cm^{-1}, with 16 scans per sample. The background of the instrument was an ambient atmosphere for all analyzed samples.

Computational Methodology. All KS-DFT calculations were performed using the ORCA program.[66] To study the GO morphologies, model clusters of graphene with different sizes and different oxygen functional groups were generated. Edges of the cluster model were terminated by hydrogen atoms so as to have a stable GO morphology with a singlet spin state. The reaction mechanisms were modeled by involving one and two GSH molecules. Figure 6 shows illustrations of reactant and product states using our cluster model. Full geometry optimizations were performed using BP86[67,68]-D3BJ[69]/def2-SVP[70] level of theory. Free energy contributions were calculated using the ideal gas, rigid rotor, and harmonic oscillator approximations at the same level of theory as the geometry optimizations. ωB97x-D3[71]/def2-TZVP single-point energy calculations were then performed on the fully optimized geometries to study the significance of high level of theory calculations. B3LYP-D3BJ/def2-TZVP and BP86-D3BJ/def2-TZVP single-point energies are shown in Table S2, but only ωB97x-D3/def2-TZVP energies are reported here as ωB97x-D3 is proven to be more accurate. Solvation effects were also modeled by performing single-point energy calculations using the conductor-like polarizable continuum model[72] solvation model, as implemented in ORCA. Finally, single-ended growing string method (GSM) calculations were used to model reaction pathways.[73−75] GSM calculations were found to not converge for some pathways, but even in these cases, GSM calculations found a reasonable starting guess that could be optimized to a valid transition-state structure having only one imaginary frequency. All transition-state structures reported in this paper were confirmed to have one imaginary frequency, and all the remaining structures (reactants, intermediate states, and products) have zero imaginary frequency.

■ ASSOCIATED CONTENT

Supporting Information

The Supporting Information is available free of charge at https://pubs.acs.org/doi/10.1021/acsami.0c11539.

Chemical reaction schematic for GSH oxidation to GSSG; ATR-FTIR spectra of P-ARGO and P-TGO600; oxidation of GSH by TGO600 under ambient DO conditions; the results of DFT calculations for all studied reaction schemes involving different oxygen groups on GO with thiol and amino groups of GSH; comparison of different levels of theories used in DFT calculations; the reaction energies from Figure 6 calculated using a continuum treatment for solvation; and the *XYZ* coordinates of the structures used in DFT calculations for Reactions 1 and 2 in Figure 6 and the G-SOH pathway (PDF)

■ AUTHOR INFORMATION

Corresponding Author

Leanne M. Gilbertson − *Department of Civil and Environmental Engineering and Department of Chemical and Petroleum Engineering, University of Pittsburgh, Pittsburgh, Pennsylvania 15261, United States;* orcid.org/0000-0003-3396-4204; Phone: (412) 624-1683; Email: leanne.gilbertson@pitt.edu

Authors

Yan Wang − *Department of Civil and Environmental Engineering, University of Pittsburgh, Pittsburgh, Pennsylvania 15261, United States;* orcid.org/0000-0002-9147-1136

Yasemin Basdogan − *Department of Chemical and Petroleum Engineering, University of Pittsburgh, Pittsburgh, Pennsylvania 15261, United States*

Tianyu Zhang − *Department of Civil and Environmental Engineering, University of Pittsburgh, Pittsburgh, Pennsylvania 15261, United States*

Ronald S. Lankone − *Department of Chemistry, Johns Hopkins University, Baltimore, Maryland 21218, United States*

Alexa N. Wallace − *Department of Chemistry, Johns Hopkins University, Baltimore, Maryland 21218, United States*

D. Howard Fairbrother − *Department of Chemistry, Johns Hopkins University, Baltimore, Maryland 21218, United States;* orcid.org/0000-0003-4405-9728

John A. Keith − *Department of Chemical and Petroleum Engineering, University of Pittsburgh, Pittsburgh, Pennsylvania 15261, United States;* orcid.org/0000-0002-6583-6322

Complete contact information is available at: https://pubs.acs.org/10.1021/acsami.0c11539

Author Contributions

L.M.G. conceived the study and formulated the theoretical approach with J.A.K. and the experimental approach with D.H.F. Y.W. performed the experiments and data analysis with assistance on the GSH experiments from T.Z and Y.B. performed the DFT calculations and their analysis. R.S.L., A.N.W., and D.H.F. performed XPS and ATR-FTIR characterization and analysis. Y.W. and Y.B. drafted the manuscript with guidance from L.M.G, J.A.K., and D.H.F.

Notes

The authors declare no competing financial interest.

‖Shared first authorship.

■ ACKNOWLEDGMENTS

The authors acknowledge generous financial support from the National Science Foundation: CBET-1709031 (L.M.G., Y.W., and D.H.F.) and CBET-1653392 (J.A.K. and Y.B.). The authors acknowledge the University of Pittsburgh Center for Research Computing for computational resources and support. L.M.G. and Y.W. also acknowledge the University of Pittsburgh Central Research Development Fund.

■ REFERENCES

(1) Reina, G.; Ruiz, A.; Murera, D.; Nishina, Y.; Bianco, A. "Ultramixing": A Simple And Effective Method To Obtain Controlled And Stable Dispersions Of Graphene Oxide In Cell Culture Media. *ACS Appl. Mater. Interfaces* **2019**, *11*, 7695−7702.

(2) Reina, G.; González-Domínguez, J. M.; Criado, A.; Vázquez, E.; Bianco, A.; Prato, M. Promises, Facts And Challenges For Graphene In Biomedical Applications. *Chem. Soc. Rev.* **2017**, *46*, 4400−4416.

(3) Rauti, R.; Medelin, M.; Newman, L.; Vranic, S.; Reina, G.; Bianco, A.; Prato, M.; Kostarelos, K.; Ballerini, L. Graphene Oxide Flakes Tune Excitatory Neurotransmission In Vivo By Targeting Hippocampal Synapses. *Nano Lett.* **2019**, *19*, 2858−2870.

(4) Lee, J.; Kim, J.; Kim, S.; Min, D.-H. Biosensors Based On Graphene Oxide And Its Biomedical Application. *Adv. Drug Delivery Rev.* **2016**, *105*, 275−287.

(5) Gilbertson, L. M.; Pourzahedi, L.; Laughton, S.; Gao, X.; Zimmerman, J. B.; Theis, T. L.; Westerhoff, P.; Lowry, G. V. Guiding The Design Space For Nanotechnology To Advance Sustainable Crop Production. *Nat. Nanotechnol.* **2020**, *15*, 801−810.

(6) Giraldo, J. P.; Wu, H.; Newkirk, G. M.; Kruss, S. Nanobiotechnology Approaches For Engineering Smart Plant Sensors. *Nat. Nanotechnol.* **2019**, *14*, 541−553.

(7) Lowry, G. V.; Avellan, A.; Gilbertson, L. M. Opportunities And Challenges For Nanotechnology In The Agri-Tech Revolution. *Nat. Nanotechnol.* **2019**, *14*, 517−522.

(8) Sanchez, V. C.; Jachak, A.; Hurt, R. H.; Kane, A. B. Biological Interactions Of Graphene-Family Nanomaterials: An Interdisciplinary Review. *Chem. Res. Toxicol.* **2012**, *25*, 15−34.

(9) Hu, X.; Zhou, Q. Health And Ecosystem Risks Of Graphene. *Chem. Rev.* **2013**, *113*, 3815−3835.

(10) Zou, X.; Zhang, L.; Wang, Z.; Luo, Y. Mechanisms Of The Antimicrobial Activities Of Graphene Materials. *J. Am. Chem. Soc.* **2016**, *138*, 2064−2077.

(11) Gilbertson, L. M.; Zimmerman, J. B.; Plata, D. L.; Hutchison, J. E.; Anastas, P. T. Designing Nanomaterials To Maximize Performance And Minimize Undesirable Implications Guided By The Principles Of Green Chemistry. *Chem. Soc. Rev.* **2015**, *44*, 5758−5777.

(12) Hutchison, J. E. Greener Nanoscience: A Proactive Approach To Advancing Applications And Reducing Implications Of Nanotechnology. *ACS Nano* **2008**, *2*, 395−402.

(13) Falinski, M. M.; Plata, D. L.; Chopra, S. S.; Theis, T. L.; Gilbertson, L. M.; Zimmerman, J. B. A Framework For Sustainable Nanomaterial Selection And Design Based On Performance, Hazard, And Economic Considerations. *Nat. Nanotechnol.* **2018**, *13*, 708.

(14) Geim, A. K. Graphene: Status And Prospects. *Science* **2009**, *324*, 1530−1534.

(15) Wang, Y.; Gilbertson, L. M. Informing Rational Design Of Graphene Oxide Through Surface Chemistry Manipulations: Properties Governing Electrochemical And Biological Activities. *Green Chem.* **2017**, *19*, 2826−2838.

(16) Perreault, F.; de Faria, A. F.; Elimelech, M. Environmental Applications Of Graphene-Based Nanomaterials. *Chem. Soc. Rev.* **2015**, *44*, 5861−5896.

(17) De Jesus, L. R.; Dennis, R. V.; Depner, S. W.; Jaye, C.; Fischer, D. A.; Banerjee, S. Inside And Outside: X-Ray Absorption Spectroscopy Mapping Of Chemical Domains In Graphene Oxide. *J. Phys. Chem. Lett.* **2013**, *4*, 3144−3151.

(18) Akhavan, O.; Ghaderi, E. Toxicity Of Graphene And Graphene Oxide Nanowalls Against Bacteria. *ACS Nano* **2010**, *4*, 5731−5736.

(19) Yang, K.; Li, Y.; Tan, X.; Peng, R.; Liu, Z. Behavior And Toxicity Of Graphene And Its Functionalized Derivatives In Biological Systems. *Small* **2013**, *9*, 1492−1503.

(20) Wang, K.; Ruan, J.; Song, H.; Zhang, J.; Wo, Y.; Guo, S.; Cui, D. Biocompatibility Of Graphene Oxide. *Nanoscale Res. Lett.* **2010**, *6*, 8.

(21) Liao, K.-H.; Lin, Y.-S.; Macosko, C. W.; Haynes, C. L. Cytotoxicity Of Graphene Oxide And Graphene In Human Erythrocytes And Skin Fibroblasts. *ACS Appl. Mater. Interfaces* **2011**, *3*, 2607−2615.

(22) Lu, C.-H.; Yang, H.-H.; Zhu, C.-L.; Chen, X.; Chen, G.-N. A Graphene Platform For Sensing Biomolecules. *Angew. Chem., Int. Ed. Engl.* **2009**, *48*, 4785−4787.

(23) Chou, S. S.; De, M.; Luo, J.; Rotello, V. M.; Huang, J.; Dravid, V. P. Nanoscale Graphene Oxide (nGO) As Artificial Receptors: Implications For Biomolecular Interactions And Sensing. *J. Am. Chem. Soc.* **2012**, *134*, 16725−16733.

(24) Safdari, F.; Raissi, H.; Shahabi, M.; Zaboli, M. DFT Calculations And Molecular Dynamics Simulation Study On The Adsorption Of 5-Fluorouracil Anticancer Drug On Graphene Oxide Nanosheet As A Drug Delivery Vehicle. *J. Inorg. Organomet. Polym. Mater.* **2017**, *27*, 805−817.

(25) Cen, W.; Hou, M.; Liu, J.; Yuan, S.; Liu, Y.; Chu, Y. Oxidation Of SO_2 And NO By Epoxy Groups On Graphene Oxides: The Role Of The Hydroxyl Group. *RSC Adv.* **2015**, *5*, 22802−22810.

(26) Keith, J. A.; Muñoz-García, A. B.; Lessio, M.; Carter, E. A. Cluster Models For Studying CO_2 Reduction On Semiconductor Photoelectrodes. *Top. Catal.* **2015**, *58*, 46−56.

(27) Boukhvalov, D. W.; Dreyer, D. R.; Bielawski, C. W.; Son, Y. W. A Computational Investigation Of The Catalytic Properties Of Graphene Oxide: Exploring Mechanisms By Using DFT Methods. *ChemCatChem* **2012**, *4*, 1844−1849.

(28) Chen, C.; Kong, W.; Duan, H.-M.; Zhang, J. Theoretical Simulation Of Reduction Mechanism Of Graphene Oxide In Sodium Hydroxide Solution. *Phys. Chem. Chem. Phys.* **2014**, *16*, 12858−12864.

(29) Guo, Y.-n.; Lu, X.; Weng, J.; Leng, Y. Density Functional Theory Study Of The Interaction Of Arginine-Glycine-Aspartic Acid With Graphene, Defective Graphene, And Graphene Oxide. *J. Phys. Chem. C* **2013**, *117*, 5708−5717.

(30) Noctor, G.; Mhamdi, A.; Chaouch, S.; Han, Y.; Neukermans, J.; Marquez-garcia, B.; Queval, G.; Foyer, C. H. Glutathione In Plants: An Integrated Overview. *Plant, Cell Environ.* **2012**, *35*, 454−484.

(31) Bannai, S.; Tateishi, N. Role Of Membrane Transport In Metabolism And Function Of Glutathione In Mammals. *J. Membr. Biol.* **1986**, *89*, 1−8.

(32) García-Castañeda, O.; Gaxiola-Robles, R.; Kanatous, S.; Zenteno-Savín, T. Circulating Glutathione Concentrations In Marine, Semiaquatic, And Terrestrial Mammals. *Mar. Mammal Sci.* **2017**, *33*, 738−747.

(33) Hasanuzzaman, M.; Nahar, K.; Anee, T. I.; Fujita, M. Glutathione In Plants: Biosynthesis And Physiological Role In Environmental Stress Tolerance. *Physiol. Mol. Biol. Plants* **2017**, *23*, 249−268.

(34) Perreault, F.; de Faria, A. F.; Nejati, S.; Elimelech, M. Antimicrobial Properties Of Graphene Oxide Nanosheets: Why Size Matters. *ACS Nano* **2015**, *9*, 7226−7236.

(35) Huang, G. G.; Han, X. X.; Hossain, M. K.; Ozaki, Y. Development Of A Heat-Induced Surface-Enhanced Raman Scattering Sensing Method For Rapid Detection Of Glutathione In Aqueous Solutions. *Anal. Chem.* **2009**, *81*, 5881−5888.

(36) Yuan, B.; Zeng, X.; Xu, C.; Liu, L.; Ma, Y.; Zhang, D.; Fan, Y. Electrochemical Modification Of Graphene Oxide Bearing Different Types Of Oxygen Functional Species For The Electro-Catalytic Oxidation Of Reduced Glutathione. *Sens. Actuators, B* **2013**, *184*, 15−20.

(37) Schafer, F. Q.; Buettner, G. R. Redox Environment Of The Cell As Viewed Through The Redox State Of The Glutathione Disulfide/Glutathione Couple. *Free Radicals Biol. Med.* **2001**, *30*, 1191−1212.

(38) Mirzahosseini, A.; Noszál, B. Species-Specific Standard Redox Potential Of Thiol-Disulfide Systems: A Key Parameter To Develop Agents Against Oxidative Stress. *Sci. Rep.* **2016**, *6*, 37596.

(39) Liu, S.; Zeng, T. H.; Hofmann, M.; Burcombe, E.; Wei, J.; Jiang, R.; Kong, J.; Chen, Y. Antibacterial Activity Of Graphite, Graphite Oxide, Graphene Oxide, And Reduced Graphene Oxide: Membrane And Oxidative Stress. *ACS Nano* **2011**, *5*, 6971−6980.

(40) Liu, X.; Sen, S.; Liu, J.; Kulaots, I.; Geohegan, D.; Kane, A.; Puretzky, A. A.; Rouleau, C. M.; More, K. L.; Palmore, G. T. R. Antioxidant Deactivation On Graphenic Nanocarbon Surfaces. *Small* **2011**, *7*, 2775−2785.

(41) Pasquini, L. M.; Sekol, R. C.; Taylor, A. D.; Pfefferle, L. D.; Zimmerman, J. B. Realizing Comparable Oxidative And Cytotoxic Potential Of Single-And Multiwalled Carbon Nanotubes Through Annealing. *Environ. Sci. Technol.* **2013**, *47*, 8775−8783.

(42) Wang, Y.; de Carvalho, N. A.; Tan, S.; Gilbertson, L. M. Leveraging Electrochemistry To Uncover The Role Of Nitrogen In The Biological Reactivity Of Nitrogen-Doped Graphene. *Environ. Sci.: Nano* **2019**, *6*, 3525−3538.

(43) Barrios, A. C.; Wang, Y.; Gilbertson, L. M.; Perreault, F. Structure−Property−Toxicity Relationships Of Graphene Oxide: Role Of Surface Chemistry On The Mechanisms Of Interaction With Bacteria. *Environ. Sci. Technol.* **2019**, *53*, 14679−14687.

(44) Gilbertson, L. M.; Goodwin, D. G., Jr; Taylor, A. D.; Pfefferle, L.; Zimmerman, J. B. Toward Tailored Functional Design Of Multi-Walled Carbon Nanotubes (MWNTs): Electrochemical And Antimicrobial Activity Enhancement Via Oxidation And Selective Reduction. *Environ. Sci. Technol.* **2014**, *48*, 5938−5945.

https://dx.doi.org/10.1021/acsami.0c11539
ACS Appl. Mater. Interfaces XXXX, XXX, XXX−XXX

(45) Pham, T. A.; Kim, J. S.; Kim, J. S.; Jeong, Y. T. One-Step Reduction Of Graphene Oxide With L-Glutathione. *Colloids Surf., A* **2011**, *384*, 543−548.
(46) Zheng, S.; Pfaendtner, J. Enhanced Sampling Of Chemical And Biochemical Reactions With Metadynamics. *Mol. Simul.* **2015**, *41*, 55−72.
(47) Heppner, D. E.; Janssen-Heininger, Y. M. W.; van der Vliet, A. The Role Of Sulfenic Acids In Cellular Redox Signaling: Reconciling Chemical Kinetics And Molecular Detection Strategies. *Arch. Biochem. Biophys.* **2017**, *616*, 40−46.
(48) Lim, J. C.; Choi, H.-I.; Park, Y. S.; Nam, H. W.; Woo, H. A.; Kwon, K.-S.; Kim, Y. S.; Rhee, S. G.; Kim, K.; Chae, H. Z. Irreversible Oxidation Of The Active-Site Cysteine Of Peroxiredoxin To Cysteine Sulfonic Acid For Enhanced Molecular Chaperone Activity. *J. Biol. Chem.* **2008**, *283*, 28873−28880.
(49) Chou, H.-C.; Chan, H.-L. Effect Of Glutathione Reductase Knockdown In Response To UVB-Induced Oxidative Stress In Human Lung Adenocarcinoma. *Proteome Sci.* **2014**, *12*, 2.
(50) Al-Gaashani, R.; Najjar, A.; Zakaria, Y.; Mansour, S.; Atieh, M. A. XPS And Structural Studies Of High Quality Graphene Oxide And Reduced Graphene Oxide Prepared By Different Chemical Oxidation Methods. *Ceram. Int.* **2019**, *45*, 14439−14448.
(51) Ganguly, A.; Sharma, S.; Papakonstantinou, P.; Hamilton, J. Probing The Thermal Deoxygenation Of Graphene Oxide Using High-Resolution In Situ X-Ray-Based Spectroscopies. *J. Phys. Chem. C* **2011**, *115*, 17009−17019.
(52) Figueiredo, J. L.; Pereira, M. F. R.; Freitas, M. M. A.; Órfão, J. J. M. Modification Of The Surface Chemistry Of Activated Carbons. *Carbon* **1999**, *37*, 1379−1389.
(53) Szymański, G. S.; Karpiński, Z.; Biniak, S.; Świątkowski, A. The Effect Of The Gradual Thermal Decomposition Of Surface Oxygen Species On The Chemical And Catalytic Properties Of Oxidized Activated Carbon. *Carbon* **2002**, *40*, 2627−2639.
(54) Jiang, Y.; Raliya, R.; Fortner, J. D.; Biswas, P. Graphene Oxides In Water: Correlating Morphology And Surface Chemistry With Aggregation Behavior. *Environ. Sci. Technol.* **2016**, *50*, 6964−6973.
(55) Hou, W.-C.; Chowdhury, I.; Goodwin, D. G., Jr; Henderson, W. M.; Fairbrother, D. H.; Bouchard, D.; Zepp, R. G. Photochemical Transformation Of Graphene Oxide In Sunlight. *Environ. Sci. Technol.* **2015**, *49*, 3435−3443.
(56) Cottrell, T. L. *The Strengths of Chemical Bonds*; Academic Press, 1958.
(57) Darwent, B. d. *National Standard Reference Data Series*; Natl. Bur. Stand., 1970; pp 15−22.
(58) Basdogan, Y.; Keith, J. A. A Paramedic Treatment For Modeling Explicitly Solvated Chemical Reaction Mechanisms. *Chem. Sci.* **2018**, *9*, 5341−5346.
(59) Plata, R. E.; Singleton, D. A. A Case Study Of The Mechanism Of Alcohol-Mediated Morita Baylis−Hillman Reactions. The Importance Of Experimental Observations. *J. Am. Chem. Soc.* **2015**, *137*, 3811−3826.
(60) Gray, C. M.; Saravanan, K.; Wang, G.; Keith, J. A. Quantifying Solvation Energies At Solid/Liquid Interfaces Using Continuum Solvation Methods. *Mol. Simul.* **2017**, *43*, 420−427.
(61) Nagy, P.; Winterbourn, C. C. Redox Chemistry Of Biological Thiols. *Advances in Molecular Toxicology*; Elsevier, 2010; pp 183−222.
(62) Turell, L.; Botti, H.; Carballal, S.; Radi, R.; Alvarez, B. Sulfenic Acid—A Key Intermediate In Albumin Thiol Oxidation. *J. Chromatogr. B: Anal. Technol. Biomed. Life Sci.* **2009**, *877*, 3384−3392.
(63) Rehder, D. S.; Borges, C. R. Cysteine Sulfenic Acid As An Intermediate In Disulfide Bond Formation And Nonenzymatic Protein Folding. *Biochemistry* **2010**, *49*, 7748−7755.
(64) Carballal, S.; Radi, R.; Kirk, M. C.; Barnes, S.; Freeman, B. A.; Alvarez, B. Sulfenic Acid Formation In Human Serum Albumin By Hydrogen Peroxide And Peroxynitrite. *Biochemistry* **2003**, *42*, 9906−9914.
(65) Gilbertson, L. M.; Albalghiti, E. M.; Fishman, Z. S.; Perreault, F.; Corredor, C.; Posner, J. D.; Elimelech, M.; Pfefferle, L. D.; Zimmerman, J. B. Shape-Dependent Surface Reactivity And Antimicrobial Activity Of Nano-Cupric Oxide. *Environ. Sci. Technol.* **2016**, *50*, 3975−3984.
(66) Neese, F. The ORCA Program System. *Wiley Interdiscip. Rev.: Comput. Mol. Sci.* **2012**, *2*, 73−78.
(67) Perdew, J. P. Density-Functional Approximation For The Correlation Energy Of The Inhomogeneous Electron Gas. *Phys. Rev. B* **1986**, *33*, 8822.
(68) Becke, A. D. Density-Functional Exchange-Energy Approximation With Correct Asymptotic Behavior. *Phys. Rev. A* **1988**, *38*, 3098.
(69) Grimme, S.; Ehrlich, S.; Goerigk, L. Effect Of The Damping Function In Dispersion Corrected Density Functional Theory. *J. Comput. Chem.* **2011**, *32*, 1456−1465.
(70) Weigend, F.; Ahlrichs, R. Balanced Basis Sets Of Split Valence, Triple Zeta Valence And Quadruple Zeta Valence Quality For H To Rn: Design And Assessment Of Accuracy. *Phys. Chem. Chem. Phys.* **2005**, *7*, 3297−3305.
(71) Chai, J.-D.; Head-Gordon, M. Long-range corrected hybrid density functionals with damped atom-atom dispersion corrections. *Phys. Chem. Chem. Phys.* **2008**, *10*, 6615−6620.
(72) Takano, Y.; Houk, K. N. Benchmarking The Conductor-Like Polarizable Continuum Model (CPCM) For Aqueous Solvation Free Energies Of Neutral And Ionic Organic Molecules. *J. Chem. Theory Comput.* **2005**, *1*, 70−77.
(73) Zimmerman, P. Reliable Transition State Searches Integrated With The Growing String Method. *J. Chem. Theory Comput.* **2013**, *9*, 3043−3050.
(74) Zimmerman, P. M. Growing String Method With Interpolation And Optimization In Internal Coordinates: Method And Examples. *J. Chem. Phys.* **2013**, *138*, 184102.
(75) Zimmerman, P. M. Single-Ended Transition State Finding With The Growing String Method. *J. Comput. Chem.* **2015**, *36*, 601−611.

https://dx.doi.org/10.1021/acsami.0c11539
ACS Appl. Mater. Interfaces XXXX, XXX, XXX−XXX